38. Radical Impurity Mechanisms for Helium Incorporation into Buckminsterfullerene

by **Serguei Patchkovskii** and **Walter Thiel***

Organisch-chemisches Institut, Universität Zürich, Winterthurerstrasse 190, CH-8057 Zürich

(18.XII.96)

Radical impurity mechanisms for incorporating He into C_{60} have been examined by semiempirical (MNDO) and density functional (BLYP/3-21G) calculations. The key step in these mechanisms is the insertion of He into $C_{60}X$ or $C_{60}X_2$ intermediates generated by adding the impurity X to C_{60} (X = H, Me in our model study). Contrary to C_{60}, several window-type structures with one broken C,C bond exist as local minima on the MNDO potential surfaces of $C_{60}X$ and $C_{60}X_2$, but they are mechanistically irrelevant due to extremely facile ring closure. Effective activation barriers for the penetration of He through intact hexagons and various windows are reported for 65 different pathways in $C_{60}X$ and $C_{60}X_2$. Window-type transition states are stabilized significantly when there is a C–X bond involving a C-atom from the broken C,C bond. The corresponding barriers in $C_{60}X$ and $C_{60}X_2$ are much lower than in C_{60}. This provides some theoretical support for the suggested impurity mechanisms even though the computed barriers for X = H, Me are still higher than indicated by the experiment (X unknown).

Introduction. – Endohedral He@C_{60} compounds with He inside buckminsterfullerene have been generated by high-energy collisions in a mass spectrometer [1–5] and by heating C_{60} in a He atmosphere [6], preferably under high pressure [7–9]. Possible mechanisms for He incorporation into C_{60} include the direct penetration through a hexagon [5] [10–12] and the insertion through windows where one or more bonds are broken reversibly to open a temporary hole in the C_{60} cage allowing easy incorporation of guests [6], with a possible involvement of triplets through an intersystem crossing [6] [13]. In a recent computational study of these mechanisms [14], the corresponding barriers were found to exceed 200 kcal/mol for each of the 21 pathways considered in the lowest singlet and triplet state. Barriers of this magnitude can be overcome in high-energy collisions [1–5], but not in the thermal high-pressure reactions [7–9] (typically at 600°, up to 3000 atm). Therefore, these reactions must follow a different mechanism [14].

The observed yield of He@C_{60} in the high-pressure experiments is very low [7–9] (normally around 0.1%). Hard-sphere estimates of the available volume in the C_{60} cage [6], and model potential studies [15] indicate that the equilibrium yield of He@C_{60} should be much higher. The application of a suitable statistical-mechanics treatment [15] with state-of-the-art quantum-chemical potentials for He inside C_{60} leads to equilibrium yields of 10–21% under typical experimental conditions [16]. This confirms that the high-pressure reactions do not reach equilibrium and are indeed far from equilibrium. The large discrepancy between the observed yields and the predicted equilibrium yields (two orders of magnitude) may also suggest that impurities can play an important mechanistic role [14].

Experimental evidence for the importance of impurities comes from a recent study [17] of the release of noble-gas atoms from endohedral fullerene compounds. The *Arrhe-*

nius activation energy for He release from C_{60} has originally been reported [6] to be *ca.* 80 kcal/mol which would imply a similar barrier for He insertion into C_{60}, if these reactions proceed according to $He@C_{60} \rightleftharpoons He + C_{60}$ (best *ab initio* binding energy of $He@C_{60}$: 2 kcal/mol [16]. However, in the case of $Ne@C_{60}$, it has been shown recently [17] that most of the observed Ne release is due to the thermal decomposition of C_{60} which can be substantially faster if traces of trapped solvent are not removed. The rate of Ne release strongly decreases upon careful purification (sublimation) of $Ne@C_{60}$. These observations have led to the conclusion [17] that the incorporation and release processes studied [6–9] [17] require the presence of impurities, also in the case of He release [18]. This suggests a mechanism [14] [17] where radical impurities X add to the fullerene, thereby weakening the bonds in the cage and allowing an easier insertion of a noble-gas atom. The endohedral C_{60} compound could then be generated by eliminating the impurity again. In the case of He, this mechanism can be summarized as follows:

$$C_{60} \xrightarrow{+X} C_{60}X \xrightarrow{+He} He@C_{60}X \xrightarrow{-X} He@C_{60} \quad (1)$$

Since the intermediate $C_{60}X$ may be susceptible to an attack by a second radical X, there may be an alternative pathway with two additional steps:

$$C_{60} \xrightarrow{+X} C_{60}X \xrightarrow{+X} C_{60}X_2 \xrightarrow{+He} He@C_{60}X_2 \xrightarrow{-X} He@C_{60}X \xrightarrow{-X} He@C_{60} \quad (2)$$

The present paper reports a theoretical investigation of such radical impurity mechanisms using the H-atom and the Me· radical as the simplest models for an impurity (X = H, Me). Different mechanisms for He incorporation into $C_{60}X$ and $C_{60}X_2$ are studied. The results are compared with those for He insertion into C_{60} [14].

Computational Details. – The computational methods employed were the same as in [14]: MNDO with standard parameters [12] [19] and density-functional theory (DFT) [20] using the 3-21G basis set [21]. In the DFT calculations, the standard local functional [22] was augmented by nonlocal corrections for exchange [23] and correlation [24] (BLYP). Singlet states ($He + C_{60}H_2$) were described by closed-shell wave functions (MNDO, DFT). In the case of doublet states ($He + C_{60}H$), an unrestricted treatment was applied at the DFT level (UBLYP) whereas a restricted open-shell *Hartree-Fock* (ROHF) treatment [25] was chosen at the MNDO level, for reasons discussed previously [14]. In the MNDO calculations, the molecular geometries were fully optimized and characterized as minima or transition states by force-constant analysis. Single-point energy calculations at the optimized MNDO structures were carried out using BLYP. The accuracy of this computational approach has been established through comparisons with experimental data and high-level *ab initio* results [14].

The semiempirical calculations were performed using a modified MNDO94 program [26] with analytical derivatives of the half-electron ROHF energy [27]. The DFT calculations employed the GAUSSIAN94 program [28].

Results and Discussion. – The present investigation considers He insertion into five simple hydrogenated derivatives of buckminsterfullerene C_{60} (**1**), *i.e.*, into the radical $C_{60}H$ (**2**) in its doublet ground state and into the four most stable $C_{60}H_2$ isomers **3**–**6**

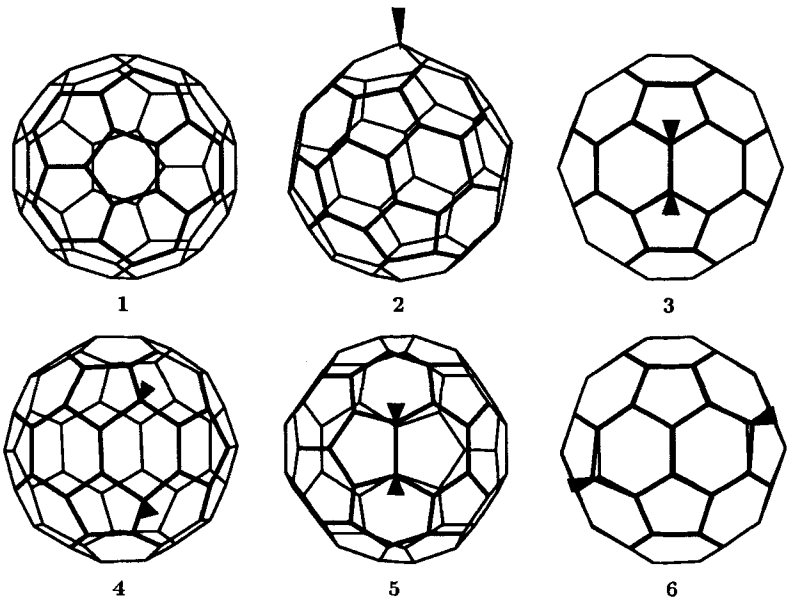

Fig. 1. *MNDO-Optimized geometries for the reference molecules.* Positions of the H-atoms are indicated by arrows.

in their singlet ground states (see *Fig. 1*). There are 23 possible $C_{60}H_2$ isomers [29] [30]. Previous calculations have established [29–31] that the most stable ones are those originating formally from C_{60} by H_2 addition to a 6-6 bond shared by two hexagons (**3**), to a hexagon in 1,4 position (**4**), to a 5-6 bond shared by a pentagon and a hexagon (**5**), and to two adjacent hexagons in 2,6 position (**6**). Both the monoadduct $C_{60}H$ (**2**) and the most stable $C_{60}H_2$ isomer (**3**) have been observed experimentally [32–34].

The analogous Me derivatives of buckminsterfullerene are also studied presently, *i.e.*, $C_{60}Me$ (**2/m**) and the corresponding $C_{60}Me_2$ isomers (**3/m**, **4/m**, **5/m**, and **6/m**). We generally adopt the notation of appending /**m** to designate the replacement of H by Me.

Table 1 lists theoretical results for the energies of these reference molecules. The MNDO and BLYP//MNDO predictions for the relative energies of the $C_{60}H_2$ isomers **3**–**6** are close to each other and to previous theoretical predictions [29–31], isomer **3** being most stable in all cases. By contrast, **4/m** is slightly favored over **3/m** (by 0.8 kcal/mol according to BLYP//MNDO), probably due to smaller steric repulsions between the Me groups in **4/m**.

It is obvious from *Table 1* that the C–H bond in $C_{60}H$ is quite weak (MNDO 55 kcal/mol, BLYP//MNDO 49 kcal/mol), and that the C–Me bond in $C_{60}CH_3$ is even weaker (MNDO 32 kcal/mol, BLYP//MNDO 37 kcal/mol). MNDO Reaction profiles indicate that the addition of H to C_{60} (**1**) requires a small barrier, which, however, disappears at the more reliable BLYP//MNDO level. The first step of the mechanism proposed in *Eqn. 1* will thus occur easily, and the activation barrier for the last step will essentially be given by the dissociation energy of the C–X bond in $C_{60}X$ (X = H, Me) which is low enough to make this step feasible under the conditions of the thermal high-pressure experiments [7–9].

Table 1. *Theoretical Results for the Reference Systems*

	Label	Point group	MNDO[a])		BLYP[b])	
			ΔH_f	E_{rel}	E_{tot}	E_{rel}
H			52.1		−0.49219	
He			0.0		−2.87628	
C_{60}	**1**	I_h	869.3		−2272.76065	
$C_{60}H$	**2**	C_s	865.9	−55.5[c])	−2273.33106	−49.1[c])
$C_{60}H_2$	**3**	C_{2v}	828.3	−89.7[d])	−2273.94815	−78.4[d])
$C_{60}H_2$	**4**	C_s	831.5	3.2[e])	−2273.94147	4.2[e])
$C_{60}H_2$	**5**	C_s	844.4	16.1[e])	−2273.92308	15.7[e])
$C_{60}H_2$	**6**	C_2	841.5	13.2[e])	−2273.92235	16.2[e])
Me		D_{3h}	25.8		−39.58856	
$C_{60}Me$	**2/m**	C_1	863.4	−31.7[f])	−2312.40734	−36.5[f])
$C_{60}Me_2$	**3/m**	C_{2v}	834.8	−54.4[g])	−2352.09222	−60.4[g])
$C_{60}Me_2$	**4/m**	C_s	826.0	−8.8[h])	−2352.09352	−0.8[h])
$C_{60}Me_2$	**5/m**	C_s	847.8	13.0[h])	−2352.07010	13.9[h])
$C_{60}Me_2$	**6/m**	C_2	836.0	1.2[h])	−2352.07735	9.3[h])

[a]) Heats of formation ΔH_f [kcal/mol] and corresponding relative energies E_{rel} [kcal/mol]. All MNDO structures are minima according to force constant analysis.

[b]) Total BLYP/3-21*G* energies E_{tot} [Hartree] and corresponding relative energies E_{rel} [kcal/mol] evaluated at MNDO optimized geometries.

[c]) Relative to C_{60} + H.

[d]) Relative to $C_{60}H$ + H.

[e]) Relative to the most stable isomer **3**.

[f]) Relative to C_{60} + Me.

[g]) Relative to $C_{60}Me$ + Me.

[h]) Relative to the isomer **3/m**.

Analogous remarks apply to the $C_{60}H_2$ isomers. Their first C–X dissociation energies are significantly higher (see *Table 1*; BLYP//MNDO: 78 kcal/mol for X = H, 60 kcal/mol for X = Me), but still small enough that the elimination steps in *Eqn. 2* are possible under typical experimental conditions [7–9].

Hence, the insertion of He into the fullerene cage is expected to be the rate-determining step both in *Eqns. 1* and *2*. Direct insertion may proceed through a hexagon or a pentagon. The latter pathway requires much more activation in the case of C_{60} [14] and will, therefore, not be considered presently. Hexagons in $C_{60}X$ and $C_{60}X_2$ which do not carry the group X should be similar to hexagons in C_{60} so that there is no need to study the direct penetration of He through these hexagons. The most favorable path should involve the insertion of He through a hexagon with a C–X bond. The corresponding transition structures are denoted by **a**, *e.g.*, **2a** in the case of He + $C_{60}H$ (see below). Due to the presence of two groups X in $C_{60}X_2$, there will generally be more than one such transition structure for the $C_{60}X_2$ isomers, which are then numbered consecutively, *e.g.*, **4a1** and **4a2** in the case of He + $C_{60}H_2$ (**4**).

Our previous study on C_{60} [14] has addressed one-bond and two-bond window mechanisms where one or two C,C bonds are broken reversibly to allow He incorporation through a temporary hole in the cage. Since the two-bond window mechanisms generally have slightly higher barriers in C_{60} [14], they will be disregarded in $C_{60}X$ and

$C_{60}X_2$. Due to symmetry, there can only be two different one-bond windows in buckminsterfullerene which are obtained by breaking a 5-6 or 6-6 bond, respectively. There are many more possibilities to generate one-bond windows in $C_{60}X$ and $C_{60}X_2$. We shall only consider one-bond windows where the group X is bound to a C-atom in the window moiety and can, therefore, assist in lowering the barrier for He insertion through such a window. This gives rise to eight distinct window structures in $C_{60}X$, five of which are formed by breaking a 5-6 bond, and three by breaking a 6-6 bond. *Fig. 2* illustrates the possible one-bond window moieties in the corresponding transition states **2b**–**2i** for He + $C_{60}X$ (**2**) and indicates the chosen labeling. The corresponding window species themselves (without He) are denoted by **2B**–**2I** (*e.g.*, **2D** corresponding to **2d**). In the case of the $C_{60}H_2$ isomers, the presence of a second group X may generate additional possibilities which will again be numbered consecutively (if necessary), *e.g.*, **4d1** and **4d2** for He + $C_{60}H_2$ (**4**).

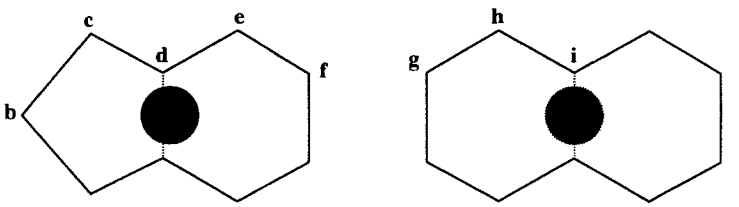

Fig. 2. *One-bond window substructures in the transition states for He + $C_{60}X$* (**2**). The position of X is denoted by **b**–**f** in the 5-6 window (left) and by **g**–**i** in the 6-6 window (right).

In C_{60}, neither 5-6 nor the 6-6 one-bond window is a local minimum on the MNDO singlet potential-energy surface [14], whereas the triplet surface is rather flat in the vicinity of the 5-6 window (no proper minimum) [14]. By contrast, four window structures have been located for $C_{60}H$ on the MNDO doublet potential-energy surface which are genuine minima according to force constant analysis (**2D**, **2E**, **2F**, **2G**; see *Fig. 3* and *Table 2*). The most stable of these species is **2D**, containing a 5-6 window with a C–H bond situated at the breaking C,C bond (68 kcal/mol above **2** according to MNDO). In the singlet $C_{60}H_2$ isomers, a low-energy window species is, therefore, expected to occur when a 5-6 window can be stabilized by two C–H bonds adjacent to the breaking C,C bond. This is indeed found: **5D** lies only 41 kcal/mol above **5** (MNDO). In the corresponding Me compounds, window structures analogous to **2D** and **5D** are also local minima on the MNDO potential surface (**2D/m** and **5D/m**, see *Table 2*).

Fig. 4 shows the MNDO reaction profiles for the formation of the window structures that have been identified in $C_{60}X$ and $C_{60}X_2$. It is obvious that the window species occupy very shallow minima on the MNDO potential surface, with barriers to ring closure which are below 5 kcal/mol in all cases (see *Table 2*). This raises the question whether they remain local minima at higher theoretical levels. BLYP Geometry optimizations of the most stable window species (**2D** and **5D**) starting from the optimized MNDO structures indeed converge to the parent compounds (**2** and **5**, resp.) indicating that **2D** and **5D** do not exist as minima on the BLYP potential surface. In any event, the window species discussed cannot be relevant mechanistically: even if they correspond to shallow minima as suggested by MNDO, they will be in rapid equilibrium with the parent

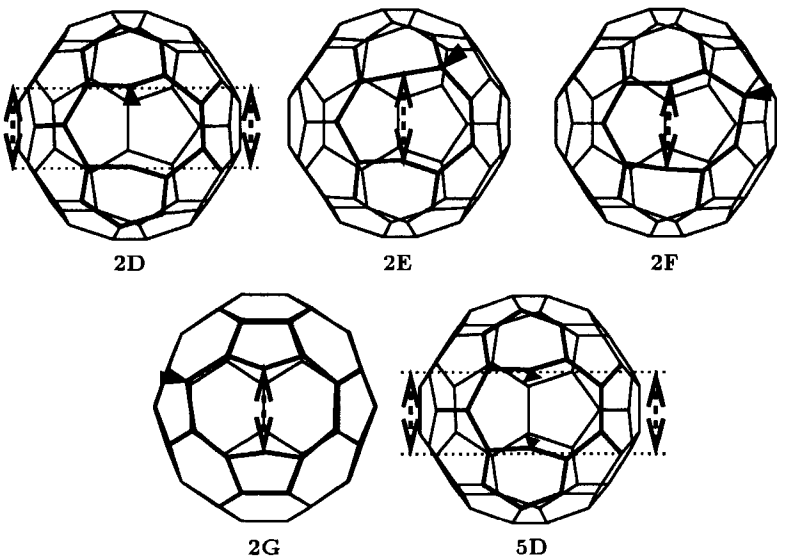

Fig. 3. *MNDO-Optimized geometries for the window structures in $C_{60}H$ and $C_{60}H_2$*. Reaction coordinates used to open the window are indicated by dashed arrows. Positions of the H-atoms are indicated by arrows.

Table 2. *Relative Energies*[a]) *for the Doublet $C_{60}X$ and Singlet $C_{60}X_2$ Window Structures and the Corresponding Transition Structures for Window Opening* (X = H, Me)

Label	Point group	Window structures			Transition structures			Remarks
		MNDO[b])	BLYP[c])	R_{C-C}[d])	MNDO[e])	BLYP[c])	R_{C-C}[d])	
Windows in $C_{60}R$								
2D	C_1	67.8	64.1[f])	2.455	69.7[g])	55.3	~ 2.260	5-6 windows
2D/m	C_1	67.4	72.8	2.560	70.9[g])	60.4	~ 2.330	
2E	C_1	119.0	118.3[h])	2.707	121.3	97.5	2.500	
2F	C_1	118.5	120.1[i])	2.686	123.2[g])	104.8	~ 2.500	
2G	C_1	134.8	138.2[j])	2.680	136.6	119.1	2.500	6-6 window
Windows in $C_{60}R_2$								
5D	C_s	40.7	32.7[k])	2.448	44.4	27.6	2.267	5-6 windows
5D/m	C_s	42.5	47.5	2.633	42.7	40.7	2.500	

[a]) Energies [kcal/mol] relative to the parent $C_{60}X$ or $C_{60}X_2$ compound, computed at the same level.
[b]) All MNDO window structures are true minima according to force constant analysis.
[c]) Single-point BLYP/3-21G calculation at the optimized MNDO geometry.
[d]) Distance [Å] between C-atoms where a bond has been broken to open the window.
[e]) All MNDO transition structures are first-order saddle points according to force constant analysis unless indicated otherwise.
[f]) BLYP/3-21G Geometry optimization starting from the optimized MNDO structure converges to **2**.
[g]) Highest point on the corresponding MNDO reaction path, not a stationary point. The orbital occupancy changes in the vicinity of this structure.
[h]) $S^2 = 0.94$
[i]) $S^2 = 0.89$.
[j]) $S^2 = 0.81$.
[k]) BLYP/3-21G Geometry optimization starting from the optimized MNDO structure converges to **5**.

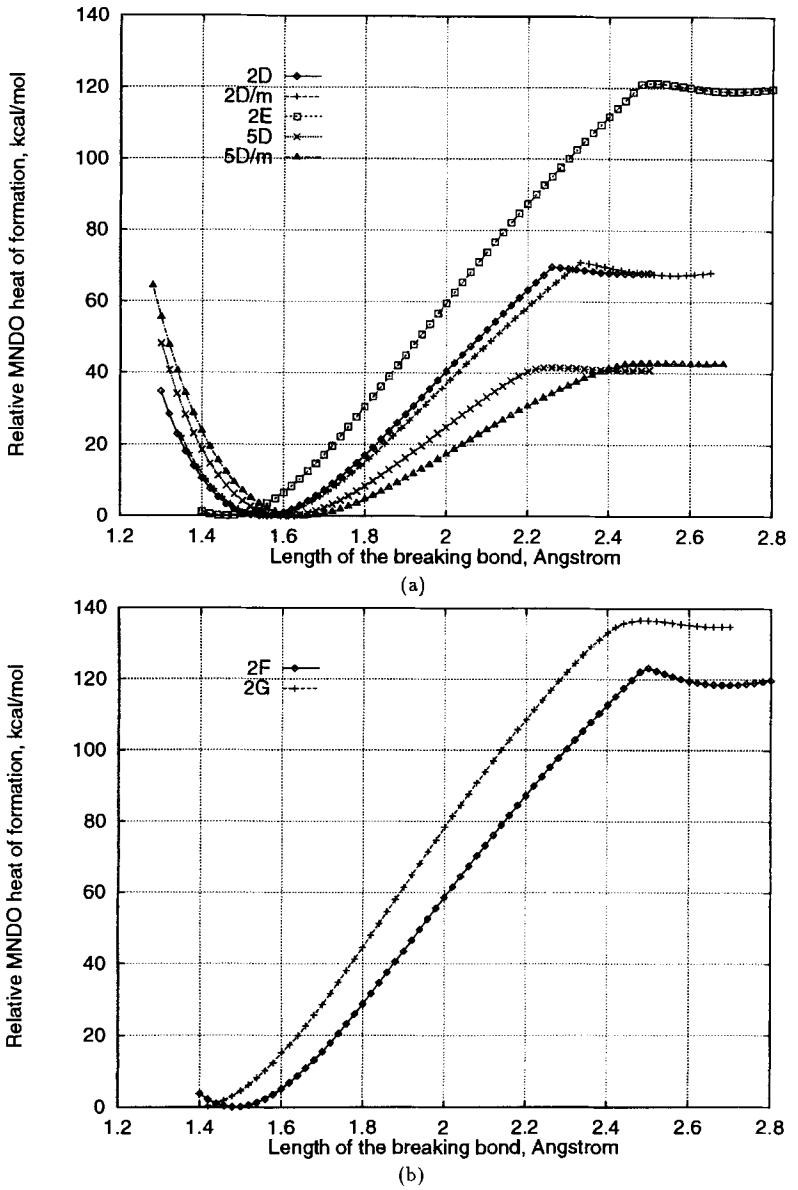

Fig. 4. *MNDO Reaction paths for window opening in $C_{60}H$* (**2D**, **2E**, **2F**, **2G**), *$C_{60}H_2$* (**5D**), *and selected $C_{60}Me$* (**2D/m**) *and $C_{60}Me_2$* (**5D/m**) *isomers*. See *Fig. 3* for definition of the reaction coordinates. Reaction coordinates for **2D/m** and **5D/m** were selected in analogy to **2D** and **5D**.

compounds under typical experimental conditions so that the activation barriers for inserting He through such a window must refer to the parent compound.

Fig. 5 shows the optimized MNDO transition structures **2a**–**2i** for He incorporation into $C_{60}H$. The corresponding activation energies are given in *Table 3*. According to

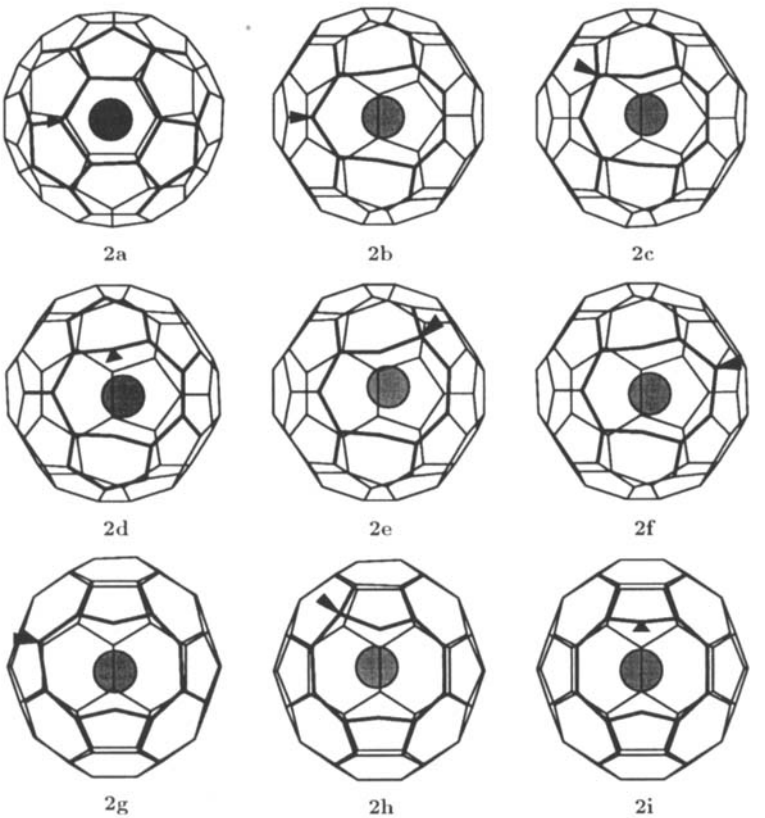

Fig. 5. *Transition structures for* $C_{60}H$ (**2**) + *He*. MNDO-Optimized geometries are shown. Positions of the H-atoms are indicated by arrows.

Table 3. *Relative Energies*[a]) *for the Doublet* $C_{60}H$ + *He Transition Structures*

Label	Point group	MNDO[b])	BLYP[c])	Label	Point group	MNDO[b])	BLYP[c])
Insertion into the intact cage				Insertion through a 6-6 one-bond window			
2a	C_1	243.4	210.0	**2g**	C_1	225.1	224.1
Insertion through a 5-6 one-bond window				**2h**	C_1	232.9	222.1[h])
2b	C_s	265.7	241.0[d])	**2i**	C_s	182.9	177.9
2c	C_1	259.3	238.7[e])				
2d	C_1	200.0	185.6[f])				
2e	C_1	213.6	215.1				
2f	C_1	226.1	223.2[g])				

[a]) Energies [kcal/mol] relative to $C_{60}H$ (**2**) with He at infinite distance, computed at the same level. [b]) All MNDO window structures are first-order saddle points according to force constant analysis. [c]) Single-point BLYP/3-21G calculation at the optimized MNDO geometry. [d]) $S^2 = 1.80$. [e]) $S^2 = 1.31$. [f]) $S^2 = 0.80$. [g]) $S^2 = 0.90$. [h]) $S^2 = 0.92$.

BLYP//MNDO it is more facile to insert He through a 6-6 window (**2i**: 178 kcal/mol) or a 5-6 window (**2d**: 186 kcal/mol) than through an intact hexagon (**2a**: 210 kcal/mol). The barriers for the window mechanisms strongly depend on the position of the H-atom (see **2b**–**2f** and **2g**–**2i**). They are lowest when the H-atom is attached to a C-atom from the C,C bond that has been broken. In the transition state, this C-atom has three σ bonds and may serve as a radical center. It is qualitatively reasonable that C–H bonds at the positions undergoing the largest change in the bonding situation (**2d**, **2i**) are more stabilizing than at other positions.

Figs. 6–9 illustrate the optimized MNDO transition structures for He insertion into the four $C_{60}H_2$ isomers considered. *Table 4* lists the associated barriers, *i.e.*, MNDO values for all reactions and selected BLYP//MNDO values for those reactions which are relatively favorable according to MNDO. Consistent with the results for $C_{60}H$, the lowest barriers are found when both C-atoms in the breaking C,C bond carry a stabilizing C–H bond. This is realized for isomer **3** in transition structure **3i** with a 6-6 window (BLYP//MNDO: 171 kcal/mol) and for isomer **5** in transition structure **5d** with a 5-6 window (BLYP//MDNO: 153 kcal/mol). The barriers for the isomers **4** and **6** without vicinal H-atoms are significantly higher than those for **3** and **5** (see *Table 4*).

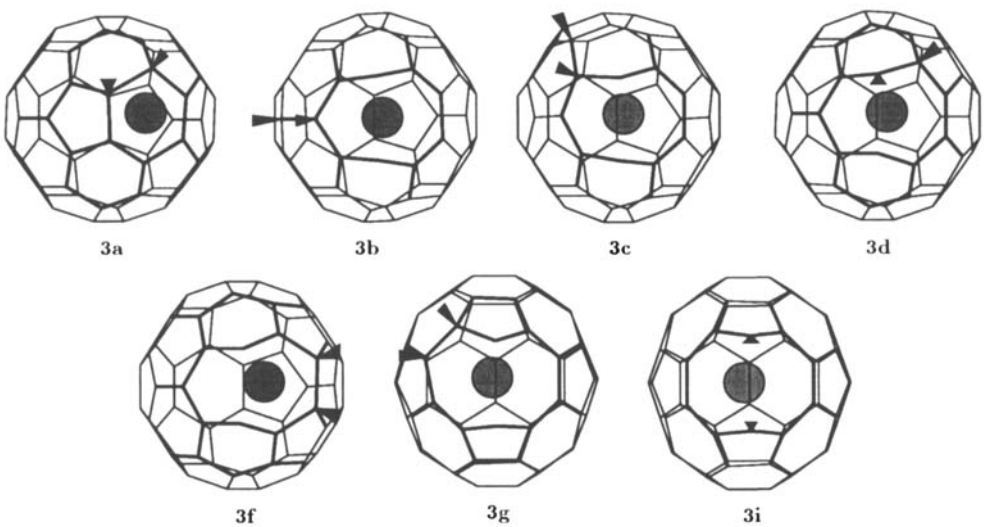

Fig. 6. *Transition structures for* $C_{60}H_2$ (**3**) + *He*. MNDO-Optimized geometries are shown. Positions of the H-atoms are indicated by arrows.

Table 5 demonstrates for selected examples how Me substitution affects the calculated MNDO barriers. In all mechanistically important cases studied, the barriers are reduced which may be rationalized by the fact that Me groups are better suited than the H-atoms to stabilize any radical centers that may be generated during the course of the reaction. In $C_{60}Me$ (**2/m**) the computed barriers are lowered by *ca.* 2, 5, and 10 kcal/mol for He insertion through an intact hexagon, a 5-6 window, and a 6-6 window, respectively. These reductions are even higher in the dimethyl compounds (up to *ca.* 20 kcal/mol in **3i/m**, see *Table 5*). This can be attributed to the presence of two stabilizing Me groups (rather than one) and partly also to the relief of steric repulsions between the vicinal Me

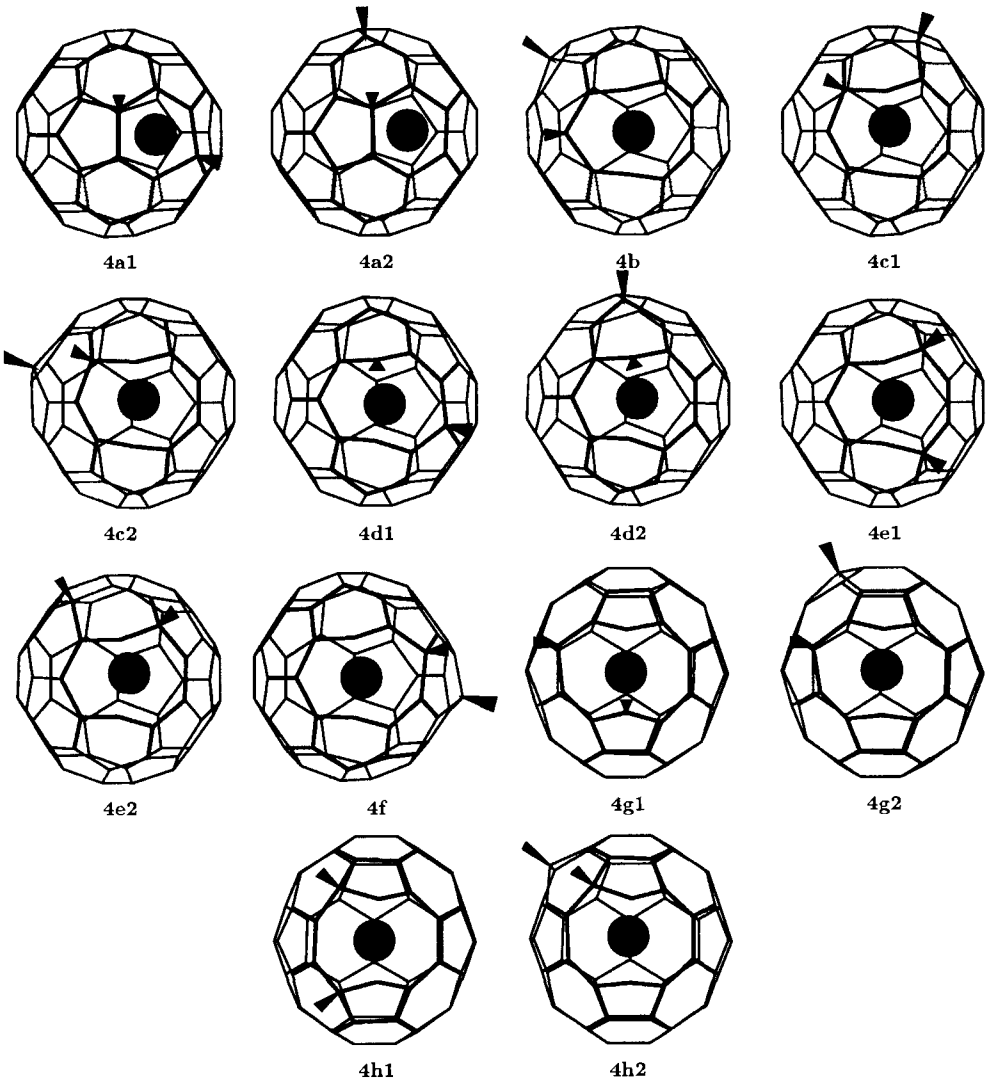

Fig. 7. *Transition structures for* $C_{60}H_2$ (**4**) + *He*. MNDO-Optimized geometries are shown. Positions of the H-atoms are indicated by arrows.

groups in **3** and **5**. Although the effects of Me substitution have only been evaluated at the MNDO level, it seems reasonable to expect similar changes in the corresponding BLYP barriers.

Table 6 compares the lowest barriers for different He insertion mechanisms in C_{60} [14], $C_{60}H$, and $C_{60}H_2$. Going from C_{60} to $C_{60}H$ lowers the computed barriers substantially, by *ca.* 20 kcal/mol for the direct insertion mechanism and *ca.* 60 kcal/mol for the window mechanisms. The transition from $C_{60}H$ to $C_{60}H_2$ leads to further reductions in the barrier, ranging approximately between 5 and 30 kcal/mol. These results confirm the

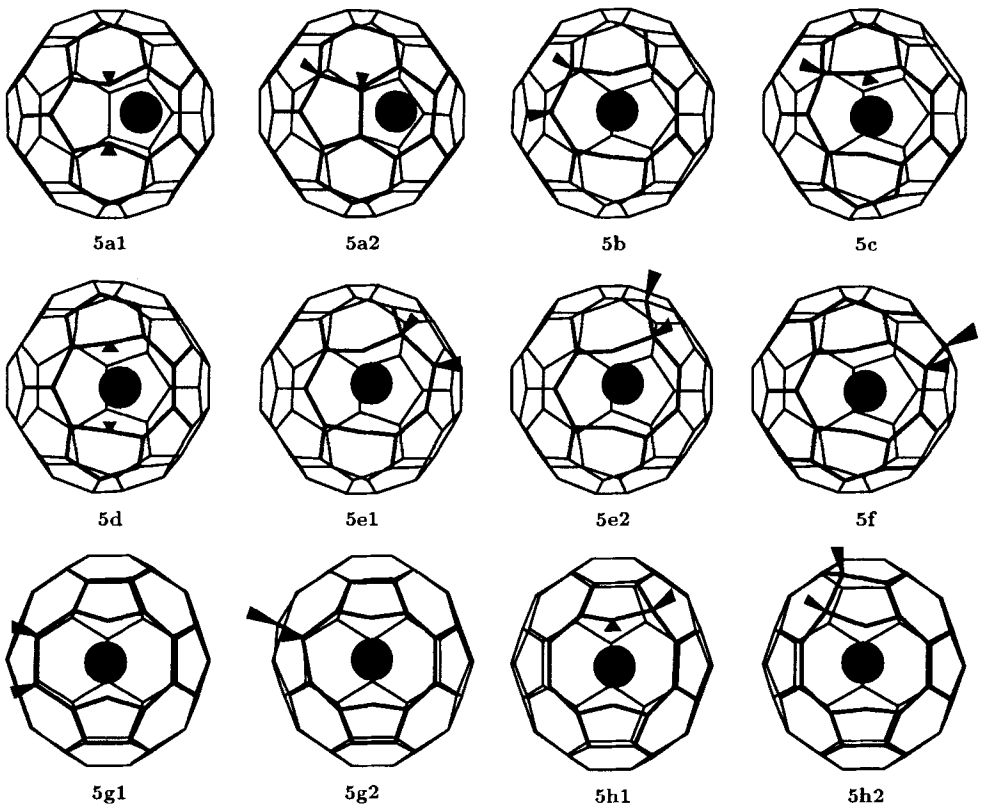

Fig. 8. *Transition structures for* $C_{60}H$ (**5**) + *He*. MNDO-Optimized geometries are shown. Positions of the H-atoms are indicated by arrows.

basic assumption of the proposed radical impurity mechanisms that He insertion into $C_{60}X$ and $C_{60}X_2$ intermediates is significantly more facile than into C_{60}, since the bonds in the fullerene cage are weakened by the addition of X.

Even in the lowest barrier in *Table 6* are still very high. Two points should be kept in mind however: first, comparison with high-level *ab initio* results for small model systems indicates [14] that our most reliable theoretical approach (BLYP//MNDO) is expected to overestimate the barriers for these insertion reactions, probably by *ca.* 10 kcal/mol or even somewhat more. Second, the barriers in *Table 6* refer to X = H and will be lower by up to 20 kcal/mol for X = Me (see *Table 5*). Taking these two factors into account yields approximate barrier estimates of *ca.* 160 and 130–140 kcal/mol for He insertion into $C_{60}Me$ and $C_{60}Me_2$, respectively. It does not seem unlikely that these barriers may still be lower for other impurities X and/or for other addition patterns.

Conclusions. – The computational exploration of a large number of insertion pathways (21 for C_{60} [14], 8 for $C_{60}H$, 49 for $C_{60}H_2$, 3 for $C_{60}Me$, and 4 for $C_{60}Me_2$) provides evidence in favor of the proposed radical impurity mechanism: the relevant barriers are much lower in $C_{60}X$ and $C_{60}X_2$ than in C_{60}, but still higher than implied by the

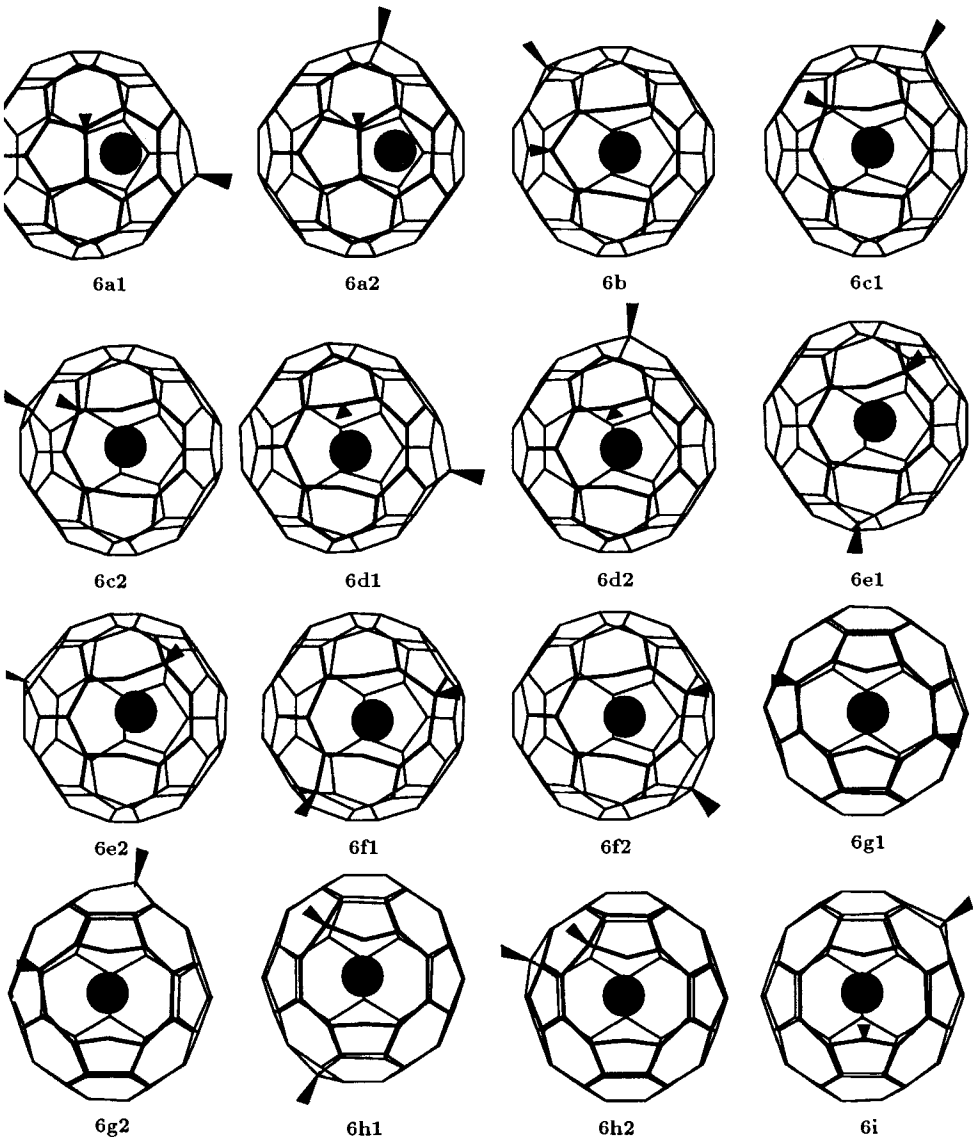

. 9. *Transition structures for* $C_{60}H_2$ (**6**) + *He*. MNDO-Optimized geometries are shown. Positions of the H-atoms are indicated by arrows.

experiment [7–9]. Further theoretical work would seem practical only when there is experimental information on the nature of the impurity X, because this would allow a targeted investigation rather than a combinatorial approach.

This work was supported by the *Swiss National Science Foundation*. Parts of the computations were performed at the Competence Center for Computational Chemistry at ETH-Zürich.

Table 4. *Relative Energies*[a]) *for the Singlet $C_{60}H_2$ + He Transition Structures*

Label	Point group	MNDO[b])	BLYP[c])	Label	Point group	MNDO[b])	BLYP[c])
Insertion into $C_{60}H_2$ (**3**)							
3a	C_s	229.8	194.5	**3b**	C_s	268.7	
3c	C_1	259.5		**3d**	C_1	234.5	187.5
3f	C_1	278.0[d])		**3g**	C_1	236.2	225.6
3i	C_s	180.1	171.4				
Insertion into $C_{60}H_2$ (**4**)							
4a1	C_s	241.3		**4a2**	C_1	242.1	
4b	C_1	267.4		**4c1**	C_1	257.0	
4c2	C_1	259.3		**4d1**	C_1	243.6	
4d2	C_1	236.6		**4e1**	C_1	231.3	211.6
4e2	C_1	257.2		**4f**	C_1	277.9	
4g1	C_1	231.9		**4g2**	C_1	236.6	
4h1	C_s	234.9		**4h2**	C_1	232.3	223.6
Insertion into $C_{60}H_2$ (**5**)							
5a1	C_s	234.6[e])	198.5	**5a2**	C_1	244.0	
5b	C_1	264.3		**5c**	C_1	235.8[d])	
5d	C_s	169.3	152.6	**5e1**	C_1	230.3	
5e2	C_1	254.5		**5f**	C_1	279.9[d])	
5g1	C_1	275.5		**5g2**	C_1	238.1	
5h1	C_1	210.0	186.5	**5h2**	C_1	232.0	
Insertion into $C_{60}H_2$ (**6**)							
6a1	C_1	247.1		**6a2**	C_1	241.5	
6b	C_1	266.0		**6c1**	C_1	257.9	
6c2	C_1	257.7		**6d1**	C_1	222.9	206.6
6d2	C_1	234.8		**6e1**	C_1	226.9	210.6
6e2	C_1	256.9		**6f1**	C_1	265.4	
6f2	C_1	277.6		**6g1**	C_1	273.5	
6g2	C_1	235.1		**6h1**	C_1	233.9	
6h2	C_1	232.8		**6i**	C_1	212.8	191.7

[a]) Energies [kcal/mol] relative to the parent $C_{60}H_2$ isomer with He at infinite distance, computed at the same level.

[b]) Unless noted otherwise, all MNDO window structures are first-order saddle points according to force constant analysis.

[c]) Single-point BLYP/3-21G calculation at the optimized MNDO geometry.

[d]) Second-order saddle point.

[e]) Second-order saddle point. The second imaginary frequency corresponds to the opening of the C(H)–C(H) bond, leading to **5d**.

Table 5. *Lowering of Activation Barriers* [kcal/mol] *upon Me Substitution*

Label	MNDO	Insertion through	Label	MNDO	Insertion through
2a/m	2.0	hexagon	**3i/m**	20.4	6-6 window
2d/m	4.7	5-6 window	**5d/m**	12.3	5-6 window
2i/m	10.3	6-6 window	**5h1/m**	11.0	6-6 window
3d/m	12.0[a])	5-6 window			

[a]) Lower limit since the structure for R = Me is a second-order saddle point.

Table 6. *Comparison of Lowest Barriers* [kcal/mol] *for He Insertion*[a])

Mechanism	Fullerene	Label	MNDO	BLYP//MNDO
Through hexagon	C_{60}	**(13s)**	265	229
	$C_{60}H$	**2a**	243	210
	$C_{60}H_2$	**3a**	230	195
Through 5-6 window	C_{60}	**(15s)**	259	252
	$C_{60}H$	**2d**	200	186
	$C_{60}H_2$	**5d**	169[b])	153[b])
Through 6-6 window	C_{60}	**(16s)**	237	235
	$C_{60}H$	**2i**	183	178
	$C_{60}H_2$	**3i**	180	171

[a]) Data for C_{60} from [14], for $C_{60}H$ from *Table 3*, and for $C_{60}H_2$ from *Table 4*. Labels for C_{60} (in parentheses) from [14].

[b]) Barriers relative to the most stable $C_{60}H_2$ isomer (**3**): MNDO 185 kcal/mol, MNDO//BLYP 168 kcal/mol.

REFERENCES

[1] T. Weiske, D. K. Böhme, J. Hrušák, W. Krätschmer, H. Schwarz, *Angew. Chem. Int. Ed.* **1991**, *30*, 884.
[2] M. M. Ross, J. H. Callahan, *J. Phys. Chem.* **1991**, *95*, 5720.
[3] K. A. Caldwell, D. E. Giblin, C. S. Hsu, D. Cox, M. L. Gross, *J. Am. Chem. Soc.* **1991**, *113*, 8519.
[4] T. Weiske, T. Wong, W. Krätschmer, J. K. Terlouw, H. Schwarz, *Angew. Chem. Int. Ed.* **1992**, *31*, 183.
[5] H. Schwarz, T. Weiske, D. K. Böhme, J. Hrušák, in 'Buckminsterfullerenes', Eds. W. E. Billups and M. A. Cuifolini, VCH, New York, 1993, pp. 257–283.
[6] M. Saunders, H. A. Jiménez-Vázquez, R. J. Cross, R. J. Poreda, *Science* **1993**, *259*, 1428.
[7] M. Saunders, H. A. Jiménez-Vázquez, R. J. Cross, S. Mroczkowski, M. L. Gross, D. E. Giblin, R. J. Poreda, *J. Am. Chem. Soc.* **1994**, *116*, 2193.
[8] M. Saunders, H. A. Jiménez-Vázquez, R. J. Cross, S. Mroczkowski, D. I. Freedberg, F. A. L. Anet, *Nature (London)* **1994**, *367*, 256.
[9] M. Saunders, R. J. Cross, H. A. Jiménez-Vázquez, R. Shimshi, A. Khong, *Science* **1996**, *271*, 1693.
[10] J. Hrušák, D. K. Böhme, T. Weiske, H. Schwarz, *Chem. Phys. Lett.* **1992**, *193*, 97.
[11] R. C. Mowrey, M. M. Ross, J. H. Callahan, *J. Phys. Chem.* **1992**, *96*, 4755.
[12] M. Kolb, W. Thiel, *J. Comput. Chem.* **1993**, *14*, 37.
[13] R. L. Murry, G. E. Scuseria, *Science* **1994**, *263*, 791.
[14] S. Patchkovskii, W. Thiel, *J. Am. Chem. Soc.* **1996**, *118*, 7164.
[15] H. A. Jiménez-Vázquez, R. J. Cross, *J. Chem. Phys.* **1996**, *104*, 5589.
[16] S. Patchkovskii, W. Thiel, *J. Chem. Phys.* **1997**, *106*, 1796.
[17] R. Shimshi, A. Khong, H. A. Jiménez-Vázquez, R. J. Cross, M. Saunders, *Tetrahedron* **1996**, *52*, 5143.
[18] M. Saunders (Department of Chemistry, Yale University, New Haven, CT 06511, USA), personal communication.
[19] M. J. S. Dewar, W. Thiel, *J. Am. Chem. Soc.* **1977**, *99*, 4899, 4907.
[20] R. G. Parr, W. Yang, 'Density-Functional Theory of Atoms and Molecules', Oxford University Press, Oxford, 1989.
[21] W. J. Hehre, L. Radom, P. v. R. Schleyer, J. A. Pople, 'Ab Initio Molecular Orbital Theory', Wiley, New York, 1986.
[22] S. H. Vosko, L. Wilk, M. Nusair, *Can. J. Phys.* **1980**, *58*, 1200.
[23] A. D. Becke, *Phys. Rev. A* **1988**, *38*, 3098.
[24] C. Lee, W. Yang, R. G. Parr, *Phys. Rev. B* **1988**, *37*, 785.
[25] M. J. S. Dewar, J. A. Hashmall, C. G. Venier, *J. Am. Chem. Soc.* **1968**, *90*, 1953.
[26] W. Thiel, Program MNDO94, version 4.0, 1994.
[27] S. Patchkovskii, W. Thiel, *Theor. Chim. Acta* **1996**, *93*, 87.

[28] M. J. Frisch, G. W. Trucks, H. B. Schlegel, P. M. W. Gill, B. G. Johnson, M. A. Robb, J. R. Cheeseman, T. Keith, G. A. Petersson, J. A. Montgomery, K. Raghavachari, M. A. Al-Laham, V. G. Zakrzewski, J. V. Ortiz, J. B. Foresman, C. Y. Peng, P. Y. Ayala, W. Chen, M. W. Wong, J. L. Andres, E. S. Replogle, R. Gomperts, R. L. Martin, D. J. Fox, J. S. Binkley, D. J. Defrees, J. Baker, J. P. Stewart, M. Head-Gordon, C. Gonzalez, J. A. Pople, GAUSSIAN94, Revision B.3, Gaussian, Inc., Pittsburgh PA, 1995.
[29] N. Matsuzawa, D. A. Dixon, T. Fukunaga, *J. Phys. Chem.* **1992**, *96*, 7594.
[30] C. C. Henderson, P. A. Cahill, *Chem. Phys. Lett.* **1992**, *198*, 570.
[31] C. C. Henderson, C. M. Rohlfing, P. A. Cahill, *Chem. Phys. Lett.* **1993**, *213*, 383.
[32] J. R. Morton, K. F. Preston, P. J. Krusic, L. B. Knight, Jr., *Chem. Phys. Lett.* **1993**, *204*, 481.
[33] C. C. Henderson, P. A. Cahill, *Science* **1993**, *259*, 1885.
[34] S. Ballenweg, R. Gleiter, W. Krätschmer, *Tetrahedron Lett.* **1993**, *34*, 3737.